13

Application of Infrared Stress Graphic System to Non-Destructive Evaluation of Composites

Sunao SUGIMOTO and Takashi ISHIKAWA

Composite Structure Section
Airframe Division
National Aerospace Laboratory

ABSTRACT

An Infrared Stress Graphic System is applied to some CFRP composites for the purpose of non-destructive evaluation. Delaminations or matrix cracks exist in these example components. It is demonstrated that this system is appropriate for in-situ non-destructive evaluation of composites. The obtained stress distribution outputs basically agree with damage patterns by other non-destructive evaluation techniques and compare favorably with the numerical results of some available cases.

1. INTRODUCTION

It is difficult to apply some non destructive evaluation (NDE) techniques to objective test pieces under in-situ conditions. However, the infrared stress measurement technique shows an advantage as an in-situ NDE method due to its optical and non-contact nature. Based on such considerations, its potential and limitations must be examined in detail. Stress distribution on the surface of a specimen under applied cyclic loading is measured using an infrared stress graphic system (ISGS) for delaminated regions and transverse cracks in CFRP laminates, as a first step. The ISGS used here is JTG-8000 made by JEOL Co. LTD. in Japan. The measured temperature fluctuation amplitude at the surface is converted into applied stress amplitude with measured thermo-elastic stress coefficient. In the case of CFRP laminates, the temperature amplitude is almost proportional to transverse stress amplitude to fiber. The measured stress distributions are compared with ultrasonic C-scan outputs and soft X-ray radiograph, and in some cases, finite element calculations. Four typical examples of stress patterns as an NDE device are demonstrated in this paper. Prior to demonstration of the experimental results the theory of the measurement is briefly reviewed.

2. BRIEF REVIEW OF INFRARED STRESS MEASUREMENT THEORY

It is common for a temperature change to be caused by pressure variation in gaseous media under adiabatic conditions. In parallel to gas, it is also caused by stress in solid continua. A linear relation between a temperature change and an applied stress must hold. However, since the temperature change is often very small in the case of solids, it cannot be observed easily. The ISGS used in this paper aims at graphic presentation of a stress distribution by means of precise measurement of the small temperature change.

The basic physical principle of this system and thermo-mechanical characteristics of CFRP laminates are described in this chapter. The first key point is that temperature variation is measured in correlation with the applied cyclic loadings. Thus, a temperature change in this measurement is identified with a temperature amplitude in one period. In the case of an isotropic solid, measured temperature amplitude corresponds to the summation of applied principle stresses. In the case of in orthotropic media, such as a CFRP ply, it can be described [1] in a plane stress state as follows :

$$dT = -\frac{T}{\rho \cdot C_\sigma}(\alpha_L \cdot d\sigma_L + \alpha_T \cdot d\sigma_T) \quad (1)$$

where

dT : Temperature variation amplitude by cyclic stresses,

T : Background temperature (in Kelvin)

ρ : Density,

C_σ : Specific heat at constant stress

α_L, α_T : Coefficient of thermal expansion (CTE) in the longitudinal (L) and transverse (T) directions

$d\sigma_L$, $d\sigma_T$: Cyclic stress amplitude in the L and T directions.

In this formulation, an irreversible temperature change caused by internal friction is neglected. By introducing two material constants, $K_{mL} = \alpha_L / (\rho \cdot C_\sigma)$, $K_{mT} = \alpha_T / (\rho \cdot C_\sigma)$, Equation (1) is rewritten as:

$$dT = -T\,(K_{mL} \cdot d\sigma_L + K_{mT} \cdot d\sigma_T) \quad (2)$$

where K_m is hereafter denoted as a thermo-elastic constant. The CTE property of CFRP, $\alpha_L << \alpha_T$, is well known [2]. Therefore, the thermo-elastic constant in the fiber direction is much smaller than the other, $K_{mL} << K_{mT}$. This means that the dT by a stress in the fiber direction is relatively small. Consequently, the measured temperature variation amplitude at a specimen surface is dominated by dT caused by a transverse stress. Thus, equation (2) can be approximated by the next equation [1].

$$dT = -K_{mT} \cdot T \cdot d\sigma_T \quad (3)$$

It is also clear that dT for the same stress amplitude are ranked as $dT_T > dT_{(45)} >> dT_L$ in cases of unidirectional (UD) CFRP.

3. BASIC MEASUREMENTS

The first step in the present method is a determination of a thermo-elastic constant, K_{mT}. Some 90 UD coupon specimens without any damage are loaded by a hydraulic testing machine, Instron 8501, in constant amplitude. Components of the ISGS system used, JTG-8000, are shown in Figure 1. This system provides us dT as a result of frame by frame computation on temperature images. Stress amplitude $d\sigma_T$ is obtained through a load cell output and room temperature data T is also required.

Before the following discussion, it should be pointed out that Equation (3) holds exactly for 90 UD. Averages of dT in defined regions on coupon surface images of 90 UD are plotted as to some levels of stress amplitude $d\sigma_X$ in Figure 2 where a suffix X denotes the loading direction. An example of dT distribution for this 90 UD is shown in Figure 2. These plotted data are best approximated by the next equation using the least square method.

$$dT = -6.58 \times 10^{-9} d\sigma_T \quad (4)$$

This equation is indicated by a solid line in Figure 2. This result and the measured room temperature $T = 298\,[\mathrm{K}]$ are substituted in Equation (3). Then, we have

$$K_T = 2.21 \times 10^{-11}\,[1 / \mathrm{Pa}] \quad (5)$$

For checking the level of approximation in Equation (3), 0 and 45 UD coupons are measured in the same way. The results are also plotted as to stress amplitudes $d\sigma_X$ in Figure 2. The results of 45 UD are converted into transverse stress amplitude and plotted by a dashed line in Figure 2. The solid and dashed lines are very close to each other. In 0 UD measurements, it is clear that $\sigma_T = 0$. Hence, the following value is obtained from the measured data and Equation (2).

$$K_L = -1.16 \times 10^{-13}\,[1 / \mathrm{Pa}] \quad (6)$$

In the following, some practical procedures related to an actual measurement is described. Temperature amplitude images by this ISGS must be accumulated and averaged to increase the signal to noise (S/N) ratio. Therefore, applied loading must be cyclic with constant amplitude and period. A schematic explanation of a relation between a temperature history at a certain surface point and applied stress variation is indicated in Figure 3. A gradual temperature change off the

applied stress frequency is eliminated as shown. According to the simplest theory described in the previous chapter, the maximum tensile stress generates the minimal temperature. In other words, the peak and bottom in a stress waveform correspond respectively to the bottom and peak in a temperature waveform. However, a time lag between the stress peak and the temperature bottom is often observed in actual measurements. This time lag leads to a phase shift between two signals. In a real measurement procedure, it is necessary to find the optimum phase shift by which an absolute value of temperature difference is maximized.

4. APPLICATION TO DELAMINATION IN CF/EPOXY LAMINATE

This ISGS system is first applied to the measurement of quasi-isotropic [(45/-45/0/90)sym.] coupon specimens of CF/Epoxy (T400/#3631) laminate under tension - tension cyclic fatigue loading. Free edge delamination starts and propagates during loading for this type of laminates due to Poisson's ratio mismatch. The loading conditions used in the tests described in this chapter are as follows: Tension-tension with stress ratio R=0.1, load control mode and constant amplitude sine wave of 5 Hz. The total area of the specimen is inspected by the ISGS and by a ultrasonic C-scanner at an appropriate interval of loadings. Applied loading level during stress measurements is maintained at a lower level than delamination propagation criticals in this area scan. When a ultrasonic C-scan inspection for monitoring delamination propagation is done, specimens are detached from the hydraulic machine used. For a trace purpose of rapidly changing delamination propagation by the ISGS, line scan inspection is used to reduce the measurement time. It should be noted that measured stress here is $d\sigma_T$, the normal stress to the fiber direction, at the surface.

Delamination onset and propagation between 0/90 and alternately 90/0 are observed in this fatigue test. These delaminations develop with increasing loading cycles and stop with a remaining strip of delamination area of 1 ~ 2 mm in width. Measured results of stress distribution transverse to loading direction by the line scan are shown in Figure 4. In order to clearly indicate C-scan edges and delamination tips symbols of | and ▲, respectively, are used in Figure 4. The measured stress pattern obtained by the area scan agrees well with an ultrasonic C-scan delamination image as indicated in Figure 5. The fact that free edge delaminations liberate surface stresses well plays a key role in such a good correlation.

Variation in stress distribution along with delamination propagation is calculated by using 20 node iso-parametric elements of a FEM software package, COMPOSIC. The true delamination experiments is located alternately appearance between in 0/90 and 90/0 interfaces as mentioned earlier. In the analysis, however, delamination location is hypothetically specified at the central plane of 90 layers for simplicity. Computations are done only for the region of $Z \geq 0$ by virtue of the assumed symmetry. Dimensions of this model are 25 mm in width, 0.6 mm in thickness and 25 mm in length. Element numbers in the X-, Y-, Z-directions are 8, 20, 4, respectively. Mesh size is uniform in the X- and Z-directions and variable in the Y-direction. Fine pitch is employed around the delamination tips and the edges. Boundary conditions concerning delamination are assumed so that nodes on the Z=0 plane are fixed in the Z-direction except for the delaminated area. Loading is modelled by sets of conditions so that nodes on the X=0 plane are fixed in the X-direction and nodes on the X=25 plane are given specified uniform displacement in the X-direction. Stress states are computed for three delamination width ratios, 0, 40 and 92%. After reaction nodal forces in the non-delaminated model are computed for given displacements corresponding to 0.8% strain, 40% and 92% delamination models are recalculated so as to have the same total reaction forces. This procedure implies the load control mode in the real experiment. The elastic constants used are assumed based on measured elastic constants in the test coupons and listed in Table 1.

The delaminated area shows an out-of-plane deformation because the delamination violates the symmetry condition. Transverse nodal stresses to fiber, σ_T, on the top 45 layer surface (at Z=0.6) are computed along the center line. These results for the above mentioned three delamination ratios are shown in Figure 6. It can be recognized that the initial stress plateau is decayed, corresponding to delamination propagation, and that stresses drop at delamination edges. The stress

drop moves inside as the delamination propagates. Numerical results indicate the stress drop and sharp stress rise across the delamination edge. Calculated results also indicate that stress level at the center decreases when the delamination is seriously propagated. In a broad sense, experimental and numerical results qualitatively coincide well with each other. In a rigorous sense, however, the measured stress level converted by K_{mT} of the unidirectional material deviates from the predicted results to some extent. Possible causes of such deviation are now being pursued for approaching a final quantitative agreement. In summary, this ISGS can be used at least as an in-situ means of non-destructive evaluation for composite laminate if damage clearly affects the surface stress state.

5. MATRIX CRACK OBSERVATION IN CF/PI-SP LAMINATE

The second example is specimens made of CF/thermoplastic (T800/PI-SP) laminates where the main concern is how matrix cracks can be seen through the ISGS. PI-SP is a new thermoplastic resin developed by Mitui-Touatu Co. LTD. The quasi-isotropic stacking sequence is the same as in the previous chapter, (45/-45/0/90)sym. The specimen is a coupon with GFRP tabs. Loading conditions including frequency, waveform, control mode and R are also the same as the previous example. Applied loading level ($\sigma_{X\,max}$ =100MPa) during the stress measurement is again maintained at a lower level. Soft X-ray radiography is used mainly for checking matrix cracks. Frame by frame summation and average is repeated for improved S/N ratio. Thus, it takes almost twenty-five minutes to measure these specimens.

Figure 7 depicts a measured stress pattern for a cracked specimen on a surface 45 layer. Matrix crack locations are indicated by the soft X-ray picture of Figure 8. Lower stress regions are observed along the matrix crack line on the surface 45 layer in Figure 7. Thus, stress liberation in the vicinity of the matrix cracks can be visualized to some extent.

Stress distribution with the matrix crack is calculated again by using 20 node iso-parametric elements of COMPOSIC. The model size is assumed to be the same as reality and only one matrix crack is supposed to exist at the center of the surface 45 layer along the fiber direction. As in the previous chapter, symmetry is also assumed. Therefore, the FEM model implies two matrix cracks symmetrically arranged with respect to the central plane. The numerical result of this model is shown in Figure 9. This graphic data indicate a narrow strip region of reduced stress and they agree basically with experimental data.

6. DELAMINATION PATTERN IDENTIFICATION IN CF/EPOXY LAMINATE FOR CAI SPECIMENS

CF/Epoxy (AS/410) CAI specimens with impact delamination are inspected by the ISGS next. The laminate stacking sequence is quasi-isotropic, [(45/0/-45/90)6]sym.. Loading conditions are as follows: compression - compression cyclic loading, load control mode and sine waveform of one Hz with a constant amplitude. Applied nominal stress amplitude is specified between -2 and -23 MPa during stress measurement. The level of this compression peak stress is almost half that of local initial buckling stress of the delaminated region [3] and is considered to be much lower than the delamination propagation trigger.

Figure 10 shows a typical ISGS stress distribution image in an impact side. Stress deviation from a uniform level can be found in regions surrounding the impact point. Higher stress regions opposite each other around the impact correspond to regions of small thickness above the first delamination. This fact implies that compressive stresses can be carried across matrix cracks in the impact side. Figure 11 shows a typical ISGS image in a back side of the impact. Wide open matrix cracks exist in the delaminated region in the back side surface ply and they create completely separated, rather floating strips from substrate laminates. Therefore, load transferring capacity in such floating strips is almost lost even for compression. Large low stress regions in Figure 11 correspond to accumulated floating strip delaminations. These ISGS stress observations contribute to examination and evaluation of the mechanical model [3] for CAI behavior prediction.

7. INSPECTION OF CF/PEEK WING BOX WITH IMPACT DAMAGE

A CF/PEEK wing box structure with an impact delamination under fatigue loading is inspected by the ISGS system as the final example here. Dimensions of this box are 900 by 452 by 150 mm. The impact side is located in a bottom surface where compression stress dominates. Although simulated quasi-random load spectrum is used in the main fatigue tests, cyclic loadings of constant amplitude and frequency are required for the ISGS measurement. Therefore, simple constant sine loadings appearing about 10 times in the last phase in each modelled flight [4] are extracted from the loading sequence and used here. The extracted parts are cancelled in the later loading patterns.

Figure 12 depicts stress distribution on the bottom panel where a schematic illustration of the loading situation and a target area is also given. A clear impact delamination identification cannot be obtained because the delamination size is very small in this case judging from C-scan image. If delamination type damage is isolated from any free edges, its effect upon surface stress is considered to be limited. The present example looks like a typical case. Note that the ISGS data indicate stress fluctuation caused by back stiffeners. An advantage of the ISGS technique as an in-situ measurement devise of stress in structure is suggested.

8. CONCLUSIONS

An ISGS system is applied to some CFRP composite components for an NDE purpose. In CF/Epoxy coupon fatigue tests, the measured stress pattern obtained by an area scan mode agrees well with an ultrasonic C-scan delamination image. The fact that free edge delaminations liberate surface stresses well plays a key role in such good correlation. However, a slight difference can be found between calculated and measured stress levels. Possible causes of such difference are now being pursued for approaching a final quantitative agreement. In CF/PI-SP specimens, matrix crack locations are identified by lower stress regions along them and agree well with a soft X-ray picture. Higher stress regions opposite each other around the impact are found in CF/Epoxy CAI specimens and they correspond to regions of small thickness above the first delamination. Such ISGS stress data contribute to an evaluation of the mechanical model for CAI behavior. In a CF/PEEK wing box application, a clear impact delamination identification can not be obtained due to small delamination size. Relations between a delamination and free edges affect the sensitivity of the ISGS measurement. In summary, it is demonstrated that the ISGS system can be used as an in-situ NDE device for composite if damage affects the surface stress state. Some limitations and problems to be solved are also clarified. The rest of the work remains to be challenged in the future.

REFERENCES

[1] K. Kageyama: Materials Science, Vol. 26 No. 1, 1989, pp.16-21 (in Japanese).

[2] T. Ishikawa: J. Composite Materials, Vol. 12, 1978.4, pp.153-168.

[3] T.Ishikawa, S. Sugimoto, M. Matsushima and Y. Hayashi: Composite Science and Technology, VOL. 55, 1996, pp. 349-363.

[4] T.Ishikawa, Y. Hayashi, S. Sugimoto and M. Matsushima: Proceedings of 7th Japan-US Conference on Composite Materials, Kyoto Japan 1995.6, pp.433-440.

Table 1 Used Elastic Constants

E_X	120.0GPa	G_{XY}	4.62GPa
E_Y	10.4GPa	G_{YZ}	3.47GPa
E_Z	10.4GPa	G_{ZX}	4.62GPa
ν_{XY}	0.36	ν_{ZX}	0.36
ν_{YZ}	0.50		

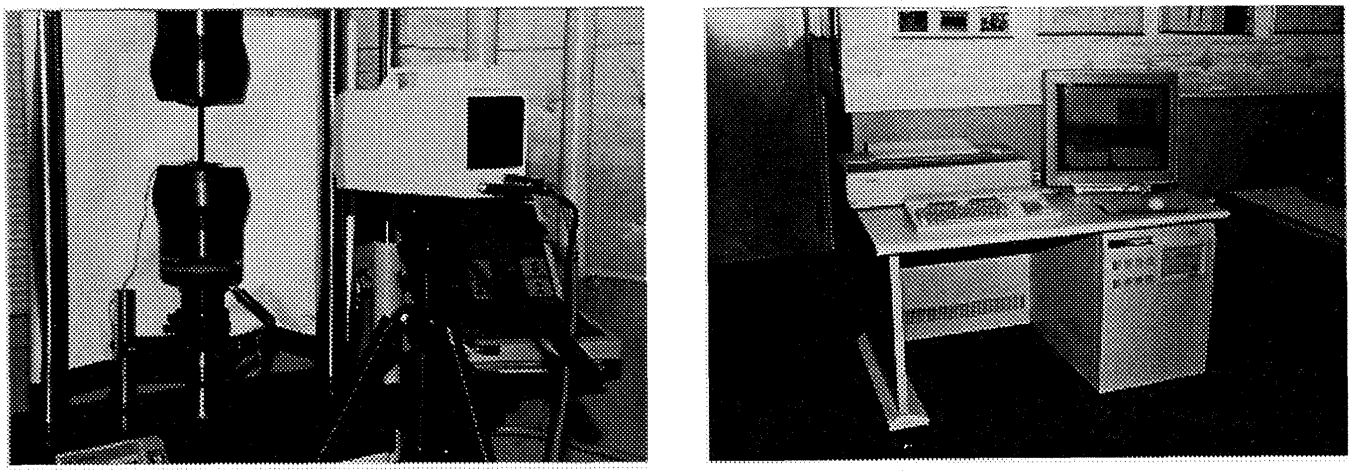

a) Sensor b) Data Processor

Figure 1 Infrared Stress Graphic System JTG-8000

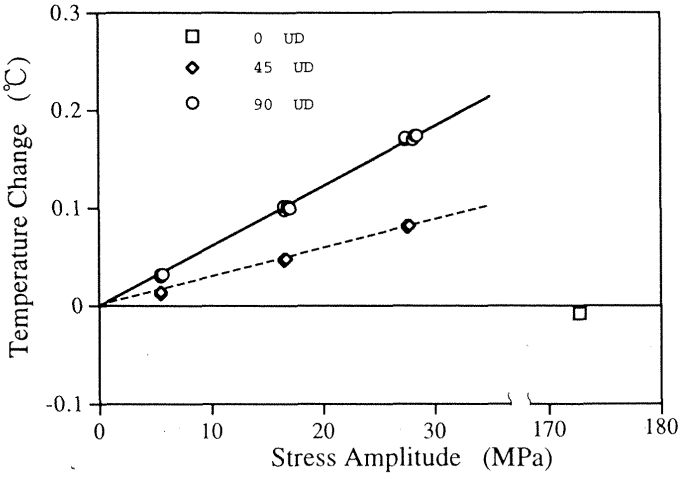

Figure 2 Relationshipsbetween dT and $d\sigma_x$

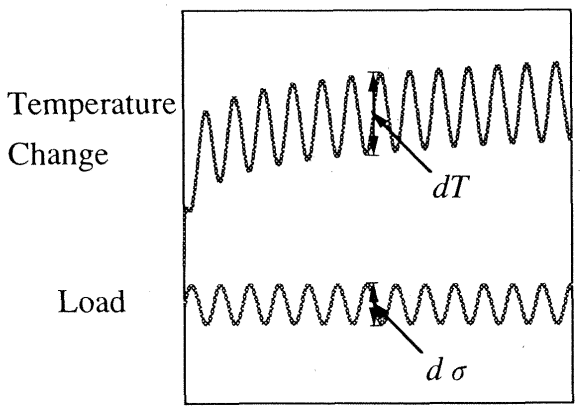

Figure 3 Schematic Situation in Temperature and Load History

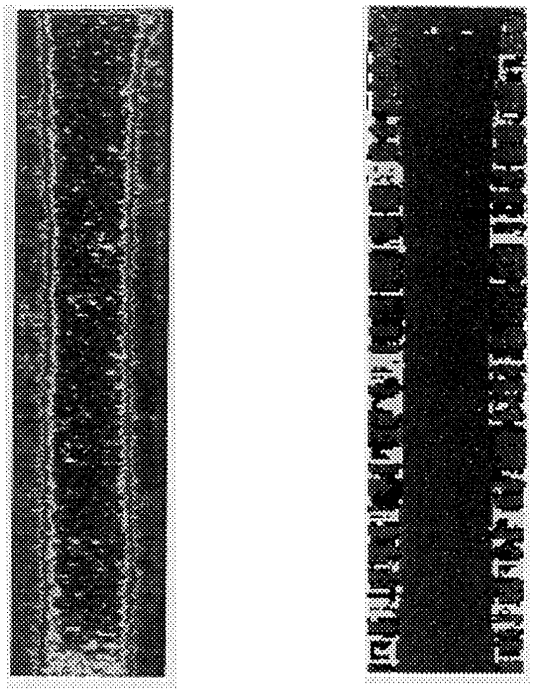

Stress Measurement C-scan Picture

Figure 4 A Comparison Measured Stress Pattern with a C-scan Result for CF/Epoxy Coupon Specimen with Edge Delamination.

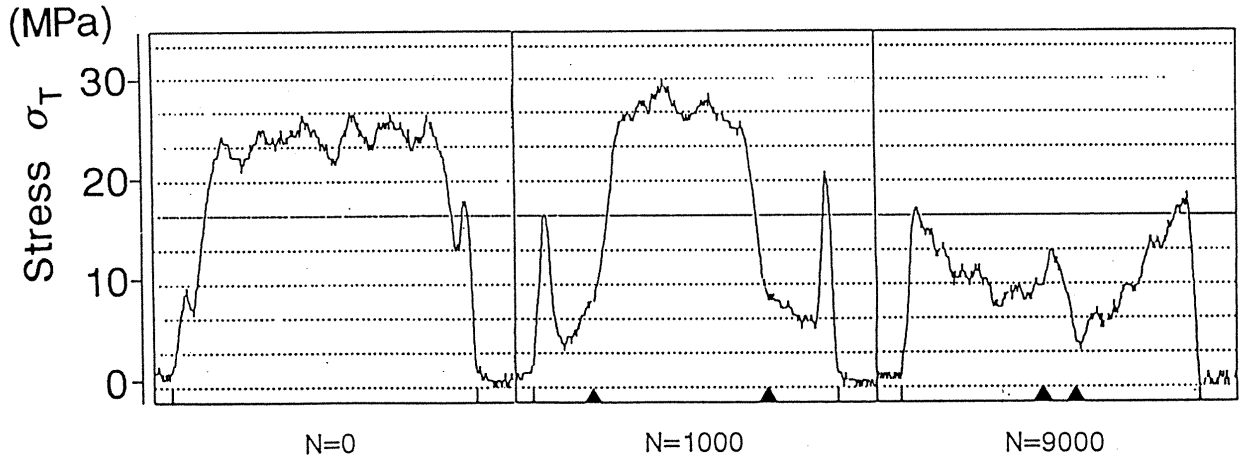

Figure 5 Measured Results of Transverse Stress on Top 45 Layer Surface

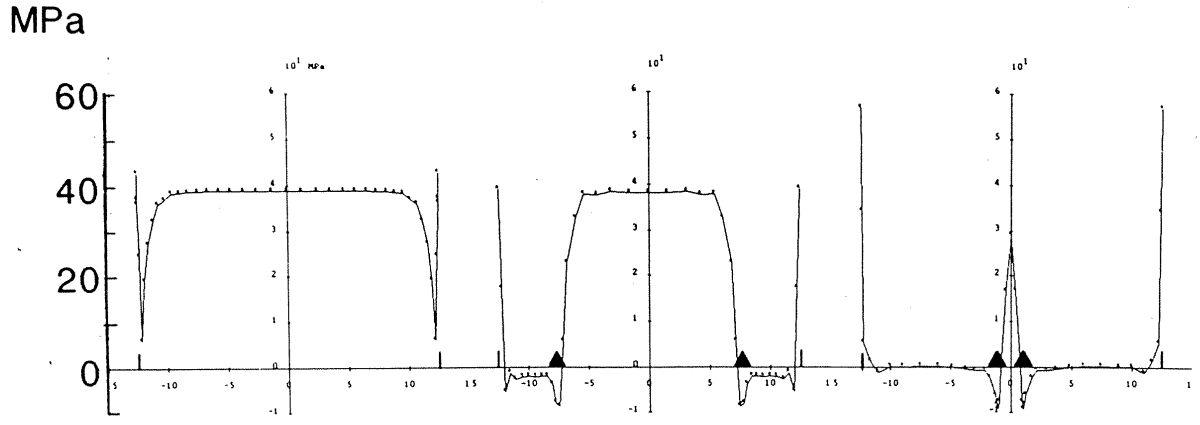

Figure 6 Numerical Results of Transverse Stresses σ_T in Top 45 Layer Surface of Delaminated Coupon

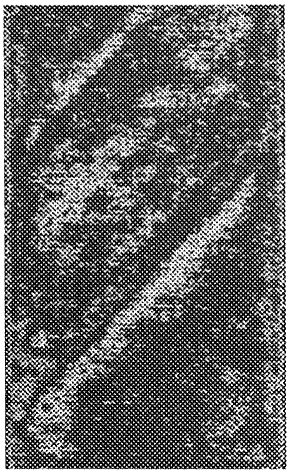

Figure 7 Measured Stress in CF/PI-SP with Matrix Cracks

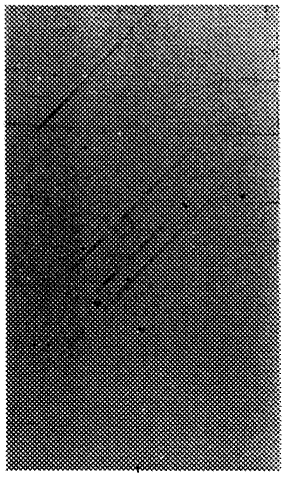

Figure 8 Soft X-ray Picture of CF/PI-SP

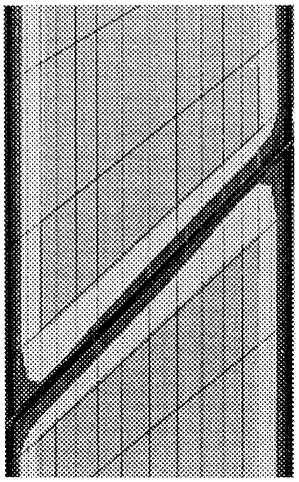

Figure 9 Numrical Sulution for CF/PI-SP with Matrix Crack

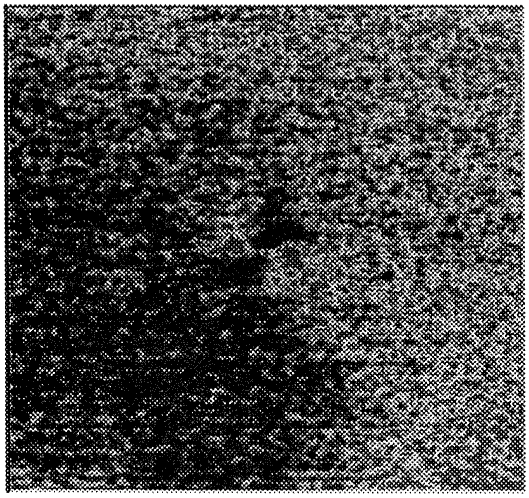

Figure 10 A Typical ISGS Result for a CF/Epoxy CAI Specimen in an Impact Side

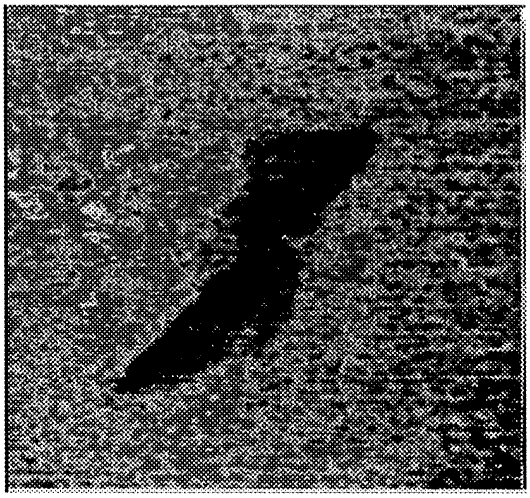

Figure 11 A Typical ISGS Result for a CF/Epoxy CAI Specimen in an Back Side

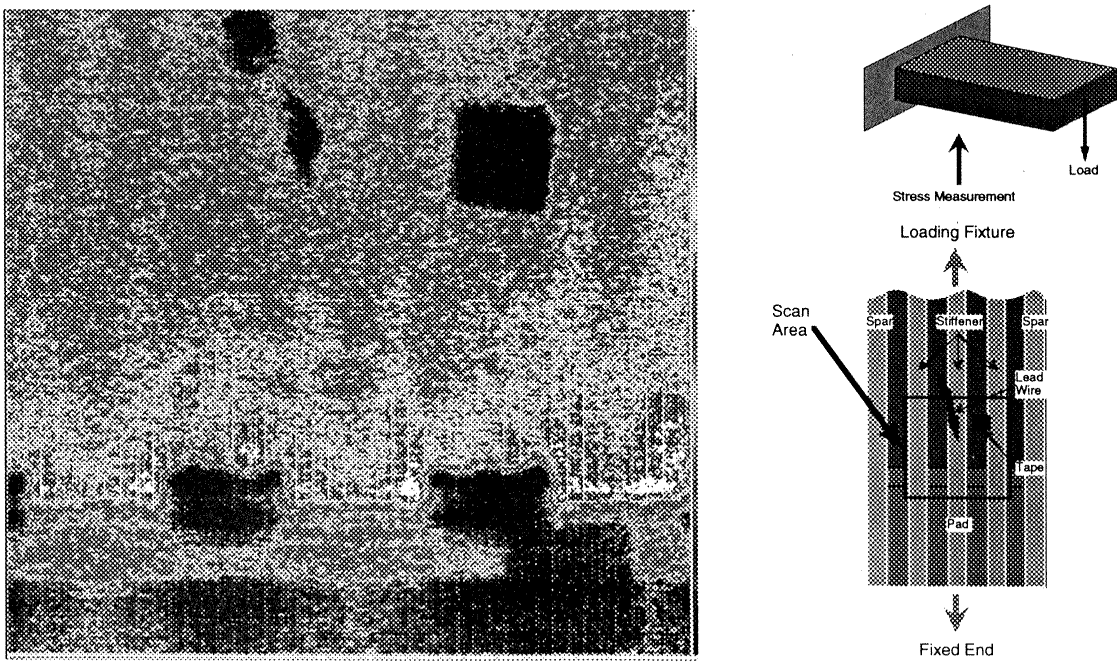

Figure 13 A Measured Stress Pattern by ISGS for a CF/PEEK Box Model with a Schematic Illustration about Scan Area.